1996

Application of Porous Electrode Theory on Metal Hydride Electrodes in Alkaline Solution

G. Zheng
University of South Carolina - Columbia

Branko N. Popov
University of South Carolina - Columbia, popov@engr.sc.edu

Ralph E. White
University of South Carolina - Columbia, white@cec.sc.edu

Publication Info

Journal of the Electrochemical Society, 1996, pages 435-441.

Publisher's link: http://dx.doi.org/10.1149/1.1836462
DOI: 10.1149/1.1836462

Editors, PV92-5, p. 3 The Electrochemical Society Proceedings Series, Pennington, NJ (1992).
14. S. R. Ovshinsky, M. A. Fetcenko, and J. Ross, *Science*, **260**, 176 (1993).
15. H. Yayama, K. Kuroki, K. Hirakawa, and A. Tomokiyo, *Jpn. J. Appl. Phys.*, **23**, 1619 (1984).
16. A. J. Bard and L. R. Faulkner, *Electrochemical Methods*, Wiley, New York (1987).
17. J. J. Borodzinski and A. Lasia, *Int. J. Hydrogen Energy*, **18**, 985 (1993).
18. D. J. Pickett, *Electrochemical Reactor Design*, Elsevier Sci. Pub. Co., Amsterdam (1979).

Application of Porous Electrode Theory on Metal Hydride Electrodes in Alkaline Solution

G. Zheng,* B. N. Popov, and R. E. White**

Department of Chemical Engineering, University of South Carolina, Columbia, South Carolina 29208, USA

ABSTRACT

Porous electrode theory was applied to estimate the exchange current density, the polarization resistance, and symmetry factor for $LaNi_{4.27}Sn_{0.24}$ hydride electrode in alkaline solution. The exchange current density, polarization resistance, and symmetry factor were determined from polarization curves which were obtained at low overpotentials.

Introduction

The performance of a metal hydride electrode is determined by the kinetics of the processes occurring at the metal-electrolyte interface and the rate of hydrogen diffusion within the bulk of the alloy.[1-8] Thus, the electrochemical kinetic properties of an electrode such as the exchange current density, polarization resistance, and the symmetry factor are important parameters which characterize the performance of the metal hydride electrode. Since the maximum hydrogen content in the alloy is of the same order as the host metal atoms,[9] it is expected that the double-layer capacity, the exchange current density, and the equilibrium potential change with the hydrogen content in the alloy. Yayama *et al.*[10] derived a concentration dependent expression for simple charge-transfer reaction and determined the dependence of the exchange current density of $TiMn_{1.5}H_x$ ($x < 0.31$) as a function of the hydrogen content in the alloy. Notten and Hokkeling[11] derived a similar concentration dependent expression for exchange current density including in the expression the influence on exchange current density by chemically adsorbed species involved in the electrochemical reaction. They measured the overall current density after 180 charge/discharge cycles and in all cases they determined a linear dependence of i *vs.* η. Exchange current values were estimated from the slope of the i *vs.* η curves at small overpotentials using a simplified Butler-Volmer equation. Ratnakumar *et al.*[12] made an attempt to correct the Tafel curves for the mass-transfer interference. However, they used the same limiting current for the cathodic and anodic portions of the curves, which obviously are different. The anodic current is limited by the hydrogen diffusion from the bulk of the alloy toward the interface, while the cathodic current is controlled by the H_2O diffusion from the bulk of the electrolyte toward the electrode/electrolyte interface. Austin[13-15] derived a general equation for the potential-current relationship for porous, flooded diffusion electrodes taking into account both the mass-transport and the ohmic effects. A Tafel region was obtained which had double the normal slope. For mass-transport restrictions in the pores of the electrode the apparent exchange current depends on the diffusion coefficient, while in the case of ohmic control in the pore electrolyte, it depends on the effective resistivity.

Here, we apply porous electrode theory to estimate the exchange current density, the polarization resistance, and symmetry factor for $LaNi_{4.27}Sn_{0.24}$ hydride electrodes in alkaline solution. The physical model originally developed by Austin[13-15] was used in the theoretical approach explained in the next section.

Porous Electrode Theory

The following steps can be distinguished during the reduction reaction on metal hydride electrode

1. The external mass transfer of water molecules from the bulk of the electrolyte to the electrode/electrolyte interface indicated by the subscripts (b) and (i), respectively

$$H_2O_{(b)} \rightleftarrows H_2O_{(i)} \qquad [1]$$

2. The internal mass transfer of water molecules from the interface of electrode/electrolyte to the pores of the electrode

$$H_2O_{(i)} \rightleftarrows H_2O_{(p)} \qquad [2]$$

where the subscript (p) represents the pore.

3. Charge-transfer reaction occurring at the surface of individual particle can be represented by

$$M + H_2O_{(p)} + e^- \underset{k^\circ_-}{\overset{k^\circ_+}{\rightleftarrows}} MH_{ads} + OH^-_{(p)} \qquad [3]$$

where k°_+ and k°_- are the reaction rate constants for the reduction and oxidation reaction, respectively.

Since the magnitude of the electrode thickness is much larger than the pore size,[13] the mass-transfer effect in the radial direction of the pores when compared to the mass transfer along the axial direction can be neglected.

4. Transport of OH^- from the pores to the interface of the electrode/electrolyte and into the bulk of the electrolyte

$$OH^-_{(p)} \rightleftarrows OH^-_{(i)} \rightleftarrows OH^-_{(b)} \qquad [4]$$

5. Hydrogen absorption

$$MH_{ads} \underset{k_{ads}}{\overset{k_{abs}}{\rightleftarrows}} MH_{abs} \qquad [5]$$

According to our studies, the hydrogen charging efficiency of the metal hydride electrode under normal charging conditions (unless it is overcharged) was close to 100%. Sakai *et al.*[8] also found high coulombic efficiencies (up to 95%) of metal hydride electrodes even at high rates (0.5 C). Consequently, the hydrogen evolution reaction may be neglected. Further, the observed 100% charging efficiency precludes the possibility that the hydrogen atom diffusion in the bulk of the alloy or the hydride formation are rate-

* Electrochemical Society Student Member.
** Electrochemical Society Active Member.

determining steps in the overall process. If either of these processes is rate determining the result is a lower charging efficiency.

Assuming that Eq. 5 is in equilibrium, and using a Langmuir isotherm for hydrogen surface coverage, one obtains

$$k_{abs}\theta\left(1-\frac{C_o}{C_s}\right) = k_{ads}(1-\theta)\frac{C_o}{C_s} \quad [6]$$

where θ is the hydrogen surface coverage, C_o is the hydrogen concentration directly beneath the surface of the electrode, and C_s is the saturation value of C_o. Equation 6 can be rearranged

$$\frac{\theta}{1-\theta} = \frac{k_{ads}C_o}{k_{abs}(C_s - C_o)} \quad [7]$$

For a one-electron transfer reaction (Eq. 3) using Langmuir isotherm for hydrogen surface coverage, the kinetic expression is

$$j' = F\left\{-k_+^o(1-\theta)C_{H_2O(p)}\exp\left[-\frac{\beta FE}{RT}\right] + k_-^o\theta C_{OH^-(p)}\exp\left[\frac{(1-\beta)FE}{RT}\right]\right\} \quad [8]$$

where j' is the microkinetic current density, *i.e.*, the current per unit internal active surface area of the electrode, C_{H_2O} and C_{OH^-} are the concentrations of H_2O and OH^-, respectively, F is the Faraday's constant, R is the gas constant, T is absolute temperature, η is the overpotential, and β is the symmetry factor.

The microkinetic exchange current density, j_o' is defined at the equilibrium potential where the external current is zero. Introducing the exchange current density into Eq. 8 results in the following current density expression

$$j' = j_o'\left\{-\frac{(1-\theta)}{(1-\theta^e)}\frac{C_{H_2O(p)}}{C^e_{H_2O(p)}}\exp\left[-\frac{\beta F\eta}{RT}\right] + \frac{\theta}{\theta^e}\frac{C_{OH^-(p)}}{C^e_{OH^-(p)}}\exp\left[\frac{(1-\beta)F\eta}{RT}\right]\right\} \quad [9]$$

where θ^e, $C^e_{H_2O}$, and $C^e_{OH^-}$, are corresponding values at equilibrium, and $C^e_{H_2O(p)} = C^e_{H_2O(b)}$, $C^e_{OH^-(p)} = C^e_{OH^-(b)}$. If reaction 5 is in equilibrium, Eq. 7 is valid. Assuming that the hydrogen diffusion is fast and hydrogen is uniformly distributed in the particle, the hydrogen concentration C_o equals the bulk concentration of hydrogen in the particle and depends only on the state of charge (which is constant) and does not depend on the potential. C_s represents the saturated hydrogen concentration which depends only on the properties of the electrode material. Therefore, the right side of Eq. 7 is independent of potential; consequently, the hydrogen surface coverage does not depend on the potential, *i.e.*, $\theta = \theta^e$. Thus, Eq. 9 becomes

$$j' = j_o'\left\{-\frac{C_{H_2O(p)}}{C^e_{H_2O(b)}}\exp\left[-\frac{\beta F\eta}{RT}\right] + \frac{C_{OH^-(p)}}{C_{OH^-(b)}}\exp\left[\frac{(1-\beta)F\eta}{RT}\right]\right\} \quad [10]$$

For a porous electrode, a mass balance on reactants and products yields[13]

$$-j = FD_{H_2O}\frac{dC_{H_2O}}{dx} = F^2u_{OH^-}C_{OH^-}\frac{dE}{dx} - FD_{OH^-}\frac{dC_{OH^-}}{dx} \quad [11]$$

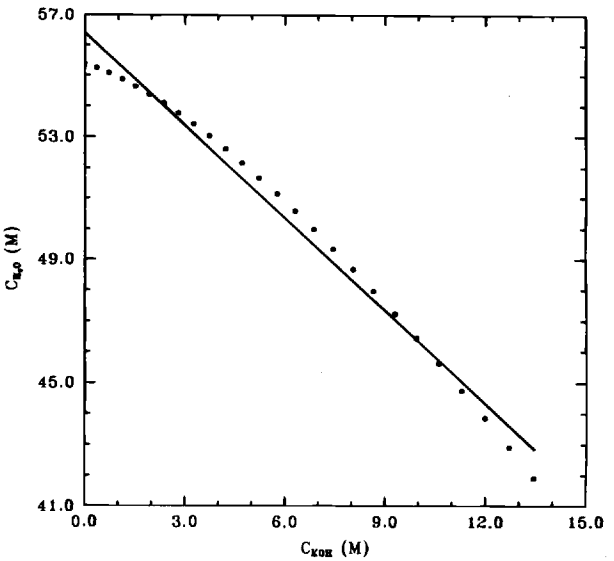

Fig. 1. Concentration relation between H_2O and KOH (from Ref. 17).

and

$$F^2u_{K^+} + C_{K^+}\frac{dE}{dx} + FD_{K^+}\frac{dC_{K^+}}{dx} = \quad [12]$$

where j is the macrokinetic current density, *i.e.*, the current per unit exposed area of the electrode, E is the potential, u_i is the ionic mobility for species i, and D_i is the effective diffusion coefficient for species i and is given by $D_i = D_i'\epsilon/\tau$, where D_i' is a mean diffusion coefficient which is close in value to the true diffusion coefficient,[14] ϵ is the porosity of the electrode, and τ is a tortuosity factor of the electrode. At higher fluxes and KOH concentrations in the pores, fluxes of H_2O and KOH may not be completely independent due to bulk flow of water in the opposite direction to the diffusion effect.[13]

Taking into account the electroneutrality

$$C_{OH^-} = C_{K^+} \quad [13]$$

Combining Eq. 11, 12, and 13, one obtains

$$D_{H_2O}\frac{dC_{H_2O}}{dx} = -\left(D_{OH^-} + \frac{u_{OH^-}}{u_{K^+}}D_{K^+}\right)\frac{dC_{OH^-}}{dx} \quad [14]$$

Substituting the Nernst-Einstein equation[16]

$$D_i = RTu_i \quad [15]$$

into Eq. 14 results in

$$D_{H_2O}\frac{dC_{H_2O}}{dx} = -2D_{OH^-}\frac{dC_{OH^-}}{dx} \quad [16]$$

Note that the Nernst-Einstein equation is applicable in dilute solution. However, for the sake of algebraic simplicity, the Nernst-Einstein equation was applied here.

In Fig. 1, the values of C_{H_2O} obtained from literature[17] are plotted as a function of C_{KOH} for KOH water solution at 25°C. As shown in Fig. 1 an approximate linear relationship holds with data regression

$$C_{H_2O} = 56.5 - 1.00C_{KOH} \quad [17]$$

Since $C_{KOH} = C_{OH^-}$, combining Eq. 17 and Eq. 16 yields

$$D_{H_2O} = 2D_{OH^-} \quad [18]$$

According to Eq. 11, a mass balance on the element dx[13,14] is

$$-dj = FD_{H_2O}\frac{d^2C_{H_2O(p)}}{dx^2}dx \quad [19]$$

The kinetic expression gives

$$dj = j'Sdx = \frac{j_o}{L}\left\{-\frac{C_{H_2O(p)}}{C_{H_2O(b)}}\exp\left[-\frac{\beta F\eta}{RT}\right] + \frac{C_{OH^-(p)}}{C_{OH^-(b)}}\exp\left[\frac{(1-\beta)F\eta}{RT}\right]\right\}dx \quad [20]$$

where j_o is the macrokinetic exchange current density, L is the half-thickness of the electrode, and S is the internal active surface area of the electrode.

From Eq. 17, we have

$$C_{H_2O(b)} + C_{OH^-(b)} = C_{H_2O(p)} + C_{OH^-(p)} \quad [21]$$

Combining Eq. 19, 20, and 21, one obtains

$$\frac{d^2C_{H_2O(p)}}{dx^2} = \frac{j_o}{FD_{H_2O}L}\left[\frac{\exp\left[-\frac{\beta F\eta}{RT}\right]}{C_{H_2O(b)}} + \frac{\exp\left[-\frac{(1-\beta)F\eta}{RT}\right]}{C_{OH^-(b)}}\right]C_{H_2O(p)} - \frac{j_o}{FD_{H_2O}L}\frac{C_{H_2O(b)}+C_{OH^-(b)}}{C_{OH^-(b)}}\exp\left[\frac{(1-\beta)F\eta}{RT}\right] \quad [22]$$

The boundary conditions are

$$\frac{dC_{H_2O(p)}}{dx} = 0 \quad at\ x = 0 \quad [23]$$

and

$$C_{H_2O(p)} = C_{H_2O(i)} \text{ at } x = L \quad [24]$$

A similar equation was solved previously by Austin.[13,14]

For negligible ohmic voltage drop in the pore electrolyte, the overpotential at the electrode/electrolyte interface has a constant value, η_i. Thus, using the equation $j = -FD_{H_2O}\,dC_{H_2O}/dx$ at $x = L$ for microkinetic current density, one obtains

$$j = j_o\left\{-\frac{C_{H_2O(i)}}{C_{H_2O(b)}}\exp\left[-\frac{\beta F\eta_i}{RT}\right] + \frac{C_{OH^-(i)}}{C_{OH^-(b)}}\exp\left[\frac{(1-\beta)F\eta_i}{RT}\right]\right\}\frac{\tanh\left(\sqrt{K}\right)}{\sqrt{K}} \quad [25]$$

where

$$K = \frac{j_oL}{FD_{H_2O}}\left\{\frac{\exp\left(-\frac{\beta F\eta_i}{RT}\right)}{C_{H_2O(b)}} + \frac{\exp\left(\frac{(1-\beta)F\eta_i}{RT}\right)}{C_{OH^-(b)}}\right\} \quad [26]$$

Equation 25 may be further reduced to the following two limiting cases.

1. If j_oL is small and the electrode polarization is low, then $\tanh(\sqrt{K})/(\sqrt{K}) \approx 1$, and consequently $C_{H_2O(i)} = C_{H_2O(b)}$ and $C_{OH^-(i)} = C_{OH^-(b)}$. Thus, Eq. 25 becomes

$$j = j_o\left\{-\exp\left[-\frac{\beta F\eta_i}{RT}\right] + \exp\left[\frac{(1-\beta)F\eta_i}{RT}\right]\right\} \quad [27]$$

Equation 27 indicates that for sufficient small electrode thickness, the porous electrode theory reduces to plane electrode theory at low overpotential so one may investigate the electrochemical kinetics of porous electrode by using electrochemical kinetic expressions valid for plane electrodes. Linearizing Eq. 27 for low overpotential, one obtains

$$j = j_o\frac{F\eta_i}{RT} \quad [28]$$

which is a j *vs.* η equation for a plane electrode. The polarization resistance may be determined by the equation

$$R_{ct} = \frac{RT}{Fj_o} \quad [29]$$

2. If it is assumed that j_oL and η are large, then $\tanh(\sqrt{K}) \approx 1$ and Eq. 25 is reduced to the charging process to

$$j = -\sqrt{\frac{j_oFD_{H_2O}}{L}C_{H_2O(b)}}\frac{C_{H_2O(i)}}{C_{H_2O(b)}}\exp\left(-\frac{\beta F\eta_i}{2RT}\right) \quad [30]$$

By neglecting external mass-transfer effects, Eq. 30 becomes a Tafel equation with a slope twice the normal value.

If it is assumed that the internal mass-transfer effect is negligible and Ohm's law must be applied, $j = 1/\rho\ (d\eta/dx)$, where ρ is the effective resistivity of the electrolyte, defined by $\rho = \rho'\tau/\epsilon$, where ρ' is the true resistivity. Then the equation to be solved is

$$\frac{d^2\eta}{dx^2} = \frac{\rho j_o}{L}\left\{-\frac{C_{H_2O(i)}}{C_{H_2O(b)}}\exp\left[-\frac{\beta F\eta}{RT}\right] + \frac{C_{OH^-(i)}}{C_{OH^-(b)}}\exp\left[\frac{(1-\beta)F\eta}{RT}\right]\right\} \quad [31]$$

The corresponding boundary conditions are

$$\frac{d\eta}{dx} = 0 \quad \text{at } x = 0 \quad [32]$$

and

$$\eta = \eta_o \quad \text{at } x = 0 \quad [33]$$

When the cathodic overpotential is large enough, then the anodic portion of Eq. 31 may be neglected. Assuming that ρ is constant, the solution is

$$j = -\sqrt{\frac{2j_oRT}{\beta\rho FL}\frac{C_{H_2O(i)}}{C_{H_2O(b)}}\exp\left[-\frac{\beta\eta_oF}{RT}\right]}\left\{\exp\left[-\frac{\beta(\eta_i-\eta_o)F}{RT}\right]-1\right\} \quad [34]$$

If the overpotential $(\eta_i - \eta_o)$ is large, $\exp[-\beta F(\eta_i - \eta_o)/RT] >> 1$, then Eq. 34 reduces to

$$j = -\sqrt{\frac{2j_oRT}{\beta\rho FL}\frac{C_{H_2O(i)}}{C_{H_2O(b)}}}\exp\left[-\frac{\beta F\eta_i}{2RT}\right] \quad [35]$$

Equation 35 is a Tafel equation which has double the normal slope.

If the external mass-transfer effect may be simply expressed by[13,18]

$$\frac{C_{(i)}}{C_{(p)}} = 1 - \frac{j}{j_l} \quad [36]$$

where j_l is the external mass-transfer limiting current density, then Eq. 30 and 35 may be rewritten in the conventional Tafel as

$$\eta_i = \frac{2.3\times 2RT}{\beta F}\log\left(\sqrt{\frac{i_oFD_{H_2O}A_s}{LM}C_{H_2O(b)}}\right) - \frac{2.3\times 2RT}{\beta F}\log\left(\frac{-i}{1-i/i_l}\right) \quad [37]$$

and

$$\eta_i = \frac{2.3\times 2RT}{\beta F}\log\left(\sqrt{\frac{2i_oRTA_s}{\beta\rho FLM}}\right) - \frac{2.3\times 2RT}{\beta F}\log\left(\frac{-i}{\sqrt{1-i/i_l}}\right) \quad [38]$$

For the discharging process, the corresponding equations are

$$\eta_i = -\frac{2.3 \times 2RT}{(1-\beta)F}\log\left(\sqrt{\frac{i_o F D_{OH^-} A_s}{LM}}\, C_{OH^-(b)}\right) + \frac{2.3 \times 2RT}{(1-\beta)F}\log\left(\frac{i}{1-i/i_l}\right) \quad [39]$$

and

$$\eta_i = -\frac{2.3 \times 2RT}{\beta F}\log\left(\sqrt{\frac{2 i_o RT A_s}{(1-\beta)\rho F L M}}\right) + \frac{2.3 \times 2RT}{(1-\beta)F}\log\left(\frac{i}{\sqrt{1-i/i_l}}\right) \quad [40]$$

For convenience, the microkinetic current density, (j) in Eq. 37 to 40, is expressed in terms of current density per unit mass, (i) (A/g) where A_s is the cross-sectional area of the electrode pellet and M is the total alloy mass of the electrode.

Our objective here was to check the applicability of the porous electrode theory for determination of electrochemical kinetic parameters of metal hydride electrodes. $LaNi_{4.27}Sn_{0.24}$ electrode was studied in alkaline solution using polarization techniques and the exchange current density, polarization resistance, and symmetry factor were determined using porous electrode theory.

Experimental

Preparation of metal hydride electrodes.—The alloy $LaNi_{4.27}Sn_{0.24}$ (Hydrogen Consultants, Inc.) was first crushed and ground mechanically. The resulting powder was passed through a 230 mesh sieve, which gave a particle size of less than 60 μm. A good electrical connection to the pellet was achieved through the following procedure: (*i*) a piece of platinum wire was passed several times through a platinum mesh; (*ii*) the platinum mesh and the wire were then pressed together to obtain good electrical connection; (*iii*) 200 mg $LaNi_{4.27}Sn_{0.24}$ pellet electrodes were prepared by mixing $LaNi_{4.27}Sn_{0.24}$ with 2.5% polytetrafluoroethylene (PTFE) powder (Goodfellow Corp.) followed by pressing the material in a cylindrical press. A 5/16 in. diam pellet was formed at ~300°C using a pressure of 5 ton/cm^2. It has been shown in literature that 2.5% of polymer binders is sufficient to bind the alloy particles.[19,20] The electrode porosity (0.37) was calculated using the thickness of the electrode, weights of the alloy and the PTFE, and the densities of the alloy and PTFE. Then, the electrode pellet was inserted between two pieces of Plexiglas holders with small holes on each side. A piece of Pt gauze on each side of the electrode served as a counter-electrode. The assembled electrode was immersed in an open test cell filled with a 6 *M* KOH electrolyte solution. Prior to the experiment, the alloy electrode was activated by repeating charge-discharge cycles. The capacity of the electrode after activation was ~270 mAh/g, which is consistent with the results reported in literature for similar alloys.[12] Charge-discharge characteristics and polarization studies were carried out at 25°C using the Model 342C SoftCorr System with EG&G Princeton Applied Research potentiostat/galvanostat Model 273A. The reference electrode was an Hg/HgO electrode. The contact between the working electrode and the reference electrode was maintained through a Luggin probe. The infrared (IR) drop error resulting from the resistance of the working electrode lead and alligator clip was eliminated by connecting the "sense jack" of the electrometer directly to the working electrode.

The experimental procedure is as follows: after the activation process, the electrode was charged under a constant current until the hydrogen content reached its saturated value. The linear polarization and Tafel polarization experiments were performed only after the open-circuit potential was stabilized (*i.e.*, the change in the potential was less than 1 mV for 1 h). Then, the electrode was discharged for a certain period of time and the same measurements as above were conducted. This procedure is repeated until the electrode is discharged to a desired potential. The experiments were carried out with more than one sample under the same conditions. All measured parameters such as equilibrium potentials, exchange current density, and symmetry factor were reproducible.

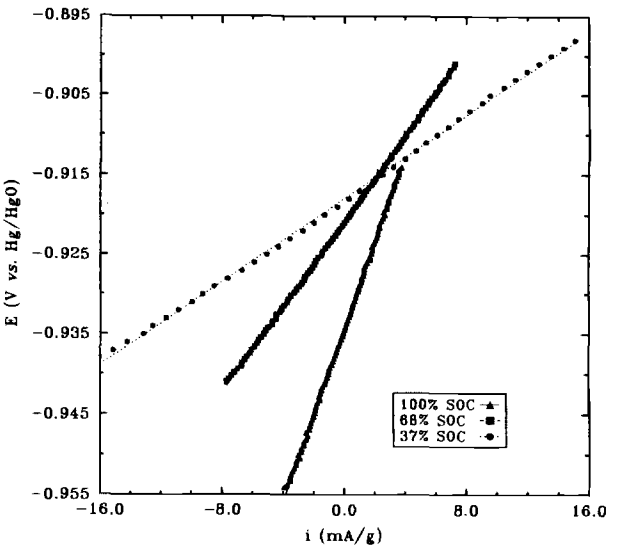

Fig. 2. Liner polorization curves (*E vs. i*) on the electrode at three different states of charge, scan rate *v* = 10 mV/s.

Results and Discussion

Comparison with experimental results.—To determine the exchange current density and polarization resistance, linear polarization curves were obtained for $LaNi_{4.27}Sn_{0.24}$ electrode in alkaline solution. Typical linear polarization curves are presented in Fig. 2. The exchange current densities were calculated from these curves using Eq. 28 and were estimated to be 4.75, 9.59, and 19.6 mA/g for 100, 68, and 37% state of charge, respectively. The polarization resistance was calculated using Eq. 29 and was 5.41, 2.68, and 1.31 Ω g, for 100, 68, and 37% state of charge, respectively.

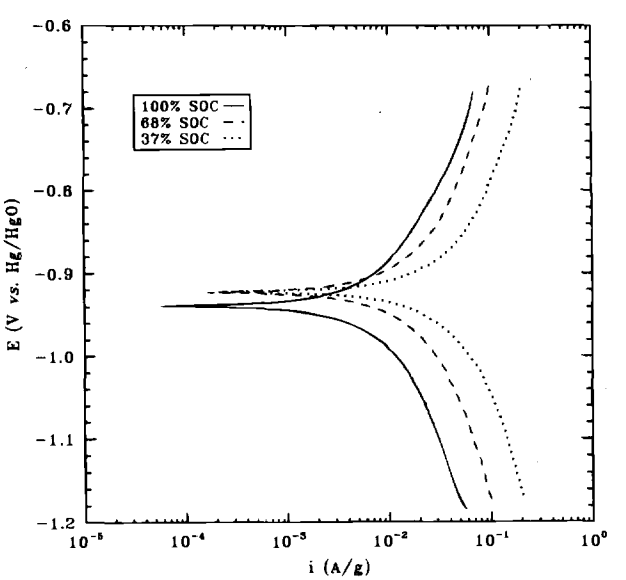

Fig. 3. Tafel plots [*E vs.* log (*i*)] on the electrode at three different states of charge, scan rate = 10 mV/s.

Tafel curves obtained for the same hydrogen content in the electrode as those used to obtain linear polarization curves in Fig. 2 are presented in Fig. 3. If a potentiostatic method was used, the corresponding current would never reach stationary state until the electrode is saturated because the hydrogen is absorbed continuously and because the equilibrium changes with time. However, we carried out Tafel experiments using a potentiodynamic method which eliminates the problem. To determine if the current is in a stationary state, initially the Tafel experiments were carried out at different scan rates (100, 10, and 1 mV/s). At this range of scan rates no obvious changes in the Tafel curves were observed indicating that the Tafel curves reached a pseudo-stationary state. Therefore, a scan rate of 10 mV/s was used to carry out the Tafel experiments. Besides the fact that they were obtained at different states of charge, the curves in Fig. 3 have the same slopes (cathodic and anodic slopes are ~360 and 330 mV/decade, respectively). In both the linear polarization studies and the Tafel experiments, we assumed that the scanning process (either in the cathodic direction or in the anodic direction) does not change the state of charge of the electrode. For instance, in Fig. 3 (at 37% state of charge of the electrode) when the potential was scanned from ~1.18 V (Hg/HgO) to ~0.92 V using a scan rate of 10 mV/s, the current density changed from −0.2 A/g to 0.2 mA/g. For this period of time (26 s), the state of charge was changed <1%. Therefore, constant state of charge is a reasonable assumption.

As discussed above, if the ohmic voltage drop through the electrode is negligible, the exchange current density and symmetry factor may be evaluated using Eq. 37 and 39, while if the internal mass-transfer effect is negligible, then the exchange current density and symmetry factor may be estimated from Eq. 38 and 40. In these equations, both limiting cases give Tafel curves twice the normal value. Consequently, from the experimental Tafel slopes it is not possible to distinguish the mass-transfer control from the ohmic control process. According to Austin,[13,14] the relative contribution of these effects depends on the parameter ϕ

$$\phi = \frac{\rho D_i F C_{i(b)} \beta}{(RT/F)} \qquad [41]$$

When $\phi > 5$, the process is ohmic controlled, when $\phi < 0.5$, the process is mass-transfer controlled. Taking $\rho = 1.6\ \Omega$ cm,[17] $D_{OH^-} = 5 \times 10^{-5}$ cm^2/s,[16] $D_{H_2O} = 2D_{OH^-} = 10^{-4}$ cm^2/s, $C_{OH^-(b)} = 6 \times 10^{-3}$ mol/cm^3, and $C_{H_2O(b)} = 51 \times 10^{-3}$ mol/cm^3,

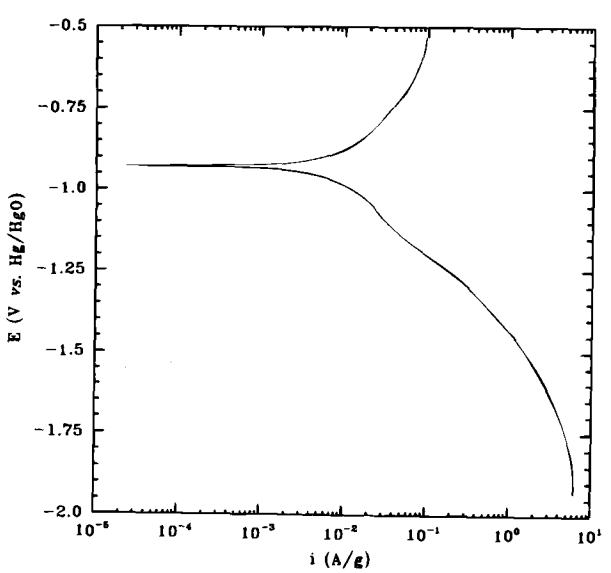

Fig. 4. A typical Tafel curve for determining the mass-transfer limiting current density on the electrode, scan rate = 10 mV/s.

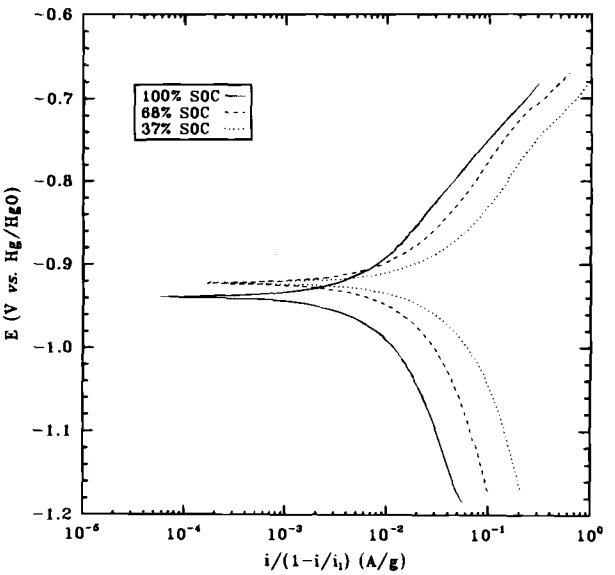

Fig. 5. Tafel curves with mass-transfer correction [E vs. log $(i/\sqrt{1 - i/i_l})$] on the electrode, scan rate = 10 mV/s.

and assuming $\beta = 0.5$, one may obtain for the charging process, $\phi = 15$, which indicates an ohmic control process while for the discharging process the same parameter was estimated to be 0.88, which indicates a mixed control process, but more on the side of a mass-transfer control process. Therefore, for the cathodic portions of the curves in Fig. 3, one may use Eq. 38 to evaluate the exchange current density and symmetry factor, while for the anodic portions of the curves, one may use Eq. 39 to estimate both kinetic parameters.

In Eq. 38 and 39, a mass-transfer limiting term exists indicating that an external mass-transfer limiting current is involved. To determine the external mass-transfer limiting current density, separate experiments were carried out in which the electrode was polarized from its equilibrium potential to about −2.0 V *vs.* Hg/HgO reference electrode in the cathodic direction and to about −0.5 V *vs.* Hg/HgO reference electrode in the anodic direction. As seen in Fig. 4, the cathodic part of the Tafel curve is far from the mass-transfer limiting region and consequently no mass-transfer corrections are necessary. However, the rate-determining step is a function of different controlling conditions. For example, for a certain charging rate, the rate-determining step may change from charge-transfer control to hydrogen diffusion control in the alloy particle when the charging time is sufficiently long so that the state of charge of the electrode changes from almost zero to close 100%. The anodic part of the Tafel curve is close to the mass-transfer region and the correction for mass-transfer is necessary. Tafel curves corrected for external mass-transfer effect (E *vs.* $i/\sqrt{1 - i/i_l}$) are presented in Fig. 5. From the cathodic branch of the Tafel curve obtained at 100% state of charge the estimated symmetry factor is about 0.34 and the corresponding apparent exchange current density ($\sqrt{2i_o RTA/\beta\rho FLM}$) for an ohmic controlled process is ~10 mA/g, which gives $i_o = 1.7 \times 10^{-2}$ mA/g. From the anodic portion of the Tafel curve, the symmetry factor was ~0.38. The apparent exchange current density ($\sqrt{i_o F D_{OH^-} A C_{OH^-(b)}/LM}$) for mass-transfer control is ~6 mA/g, which gives $i_o = 2.0 \times 10^{-2}$ mA/g. Both current densities estimated using the cathodic and anodic Tafel slopes are two orders of magnitude lower than the exchange current density values obtained using linear polarization curves (4.75 mA/g at 100% state of charge). Similar results were obtained for the other states of charge. The discrepancy in the estimation of exchange current density values indicated that it is necessary to check the validity of Eq. 39 and 38. Equation 39 holds only

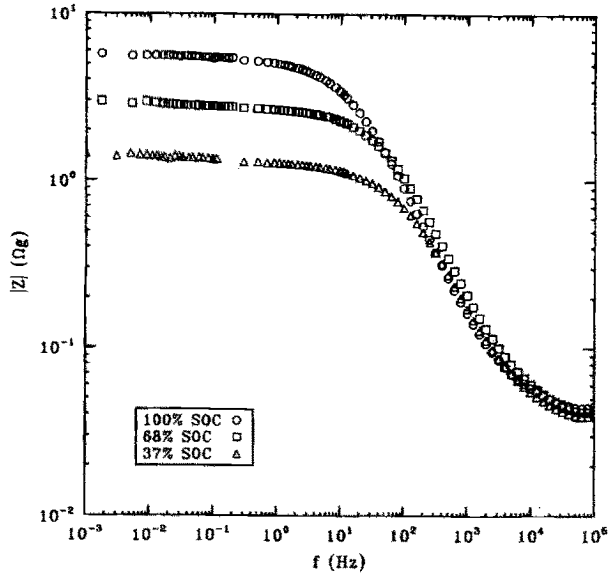

Fig. 6. Bode plots with different states of charge.

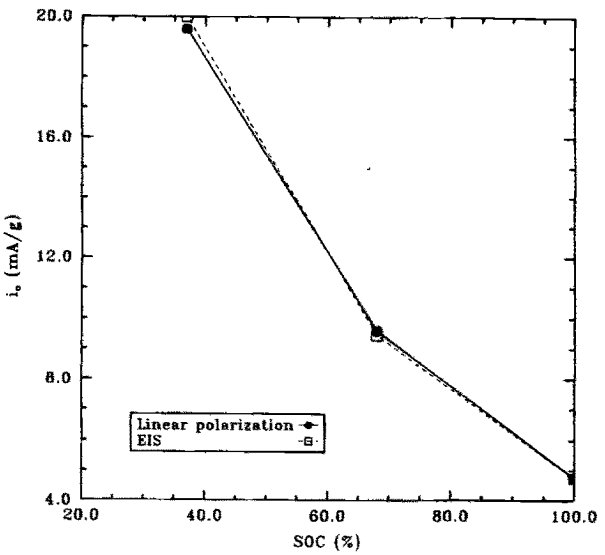

Fig. 8. Comparison of the calculated exchange current densities by linear polarization and electrochemical impedance spectroscopy technique.

when j_oL and the overpotential are high enough so K is sufficiently large to satisfy $\tanh(\sqrt{K}) \approx 1$. According to Eq. 26

$$K = \frac{i_oLM}{AFD_{OH^-}} \left\{ \frac{\exp\left[\frac{\beta F\eta_i}{RT}\right]}{C_{H_2O(b)}} + \frac{\exp\left[-\frac{(1-\beta)F\eta_i}{RT}\right]}{C_{OH^-(b)}} \right\} \quad [42]$$

and consequently K may be estimated by substituting the maximum overpotential of 0.25 V from the Tafel curve and the exchange current density obtained from the linear polarization (since it is larger), which gives $K = 9.7 \times 10^{-3}$ and $\tanh(\sqrt{K}) \approx 0.1$. Thus, Eq. 39 cannot be used to estimate the exchange current density and symmetry factor of $LaNi_{4.27}Sn_{0.24}$ hydride electrode in alkaline solution.

Equation 38 is valid only if $\exp[-\beta(\eta_i - \eta_o)F/RT] >> 1$. The overpotential drop through the electrode pellet may be estimated using Ohm's law $i = A_s/\rho M\ (d\eta/dx)$. Assuming that ρ is constant (1.6 Ω cm) through the electrode and using the maximum current density from the Tafel curve (6×10^{-2} A/g), one obtains an overpotential of $\eta_i - \eta_o \approx -1.5$ mV, which gives the exponential term exp $[-\beta F(\eta_i - \eta_o)/RT] = 1.0$, which does not satisfy the condition that $\exp[-\beta(\eta_i - \eta_o)F/RT] >> 1$. Thus, Eq. 38 cannot be used to estimate the exchange current density either. Also, for such a small potential drop, it is not reasonable to assume an ohmic control even for $\phi = 15$. Consequently, comparison of the model with the experimental results indicates that the conventional Tafel extrapolation method cannot be applied to test the metal hydride electrode and to determine the exchange current density and symmetry factor.

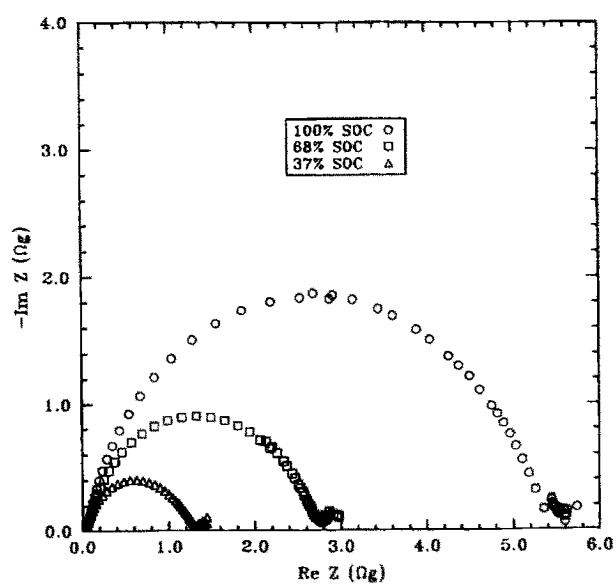

Fig. 7. Nyquist plots with different states of charge.

To check the validity of the linear polarization technique, electrochemical impedance spectroscopy (EIS) was used to determine the exchange current density as a function of different states of charge of the electrode. The Bode and Nyquist plots for three different states of charge are presented in Fig. 6 and 7. The exchange current densities were calculated using Eq. 29. The calculated exchange current densities from both linear polarization and EIS techniques are compared in Fig. 8. As shown in this figure the estimated current densities from these two techniques for different states of charge are in excellent agreement which validates the polarization technique for determination of kinetic parameters.

The original equations such as Eq. 25 and 34 may be used to estimate the electrochemical kinetic parameters such as exchange current density. However, they are not in convenient forms for evaluation of exchange current density.

The exchange current density can be determined from the linear polarization curves. However, the symmetry factor cannot be evaluated by using a linear polarization curve. To determine the symmetry factor we rearrange Eq. 27 in the terms of mass current density as

$$\frac{i}{\exp(F\eta_i/RT) - 1} = i_o \exp(-\beta F\eta_i/RT) \quad [43]$$

Taking the logarithm of Eq. 43, one obtains[18,21]

$$\eta_i = \frac{2.3RT}{\beta F} \log i_o - \frac{2.3RT}{\beta F} \log\left[\frac{i}{\exp(F\eta_i/RT) - 1}\right] \quad [44]$$

Thus, from the slope of a plot of η_i *vs.* log $[i/\exp(F\eta_i/RT) - 1]$, the symmetry factor β can be determined. Equation 44 is only valid in the linear polarization region. The experimental results shown in Fig. 2 are plotted in Fig. 9 to evaluate β. From this figure it can be seen that a linear relationship exits for η_i *vs.* log $[i/\exp(F\eta_i/RT) - 1]$. The slopes are 102, 110, and 100 mV/decade

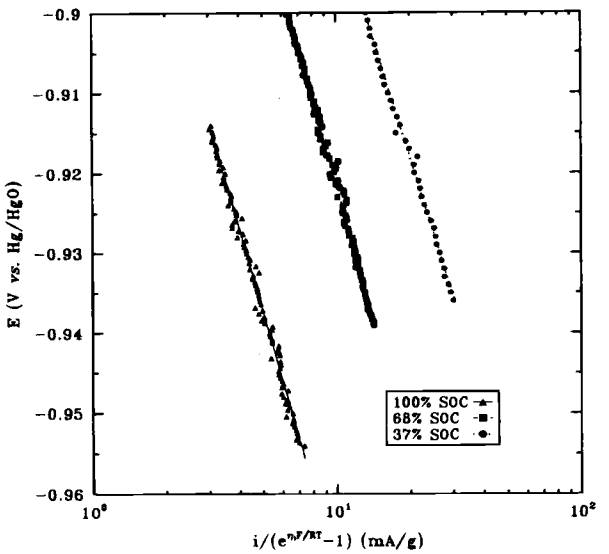

Fig. 9. Linear polarization curves {E vs. log [i/exp ($\eta_i F/RT$) − 1]} on the electrode at different states of charge, scan rate = 10 mV/s.

for 100, 68, and 37% states of charge, respectively. The average symmetry factor from the slopes is approximately 0.57.

Conclusion

Porous electrode theory was applied to estimate the exchange current density, the polarization resistance, and the symmetry factor for $LaNi_{4.27}Sn_{0.24}$ hydride electrodes in alkaline solution. Both the exchange current density and symmetry factor are evaluated from the polarization curves obtained at low overpotentials and give $\beta = 0.57$ and i_o in the range of 4.75 to 19.6 mA/g for 100 to 37% states of charge. The corresponding polarization resistances are in the range of 5.41 to 1.31 Ω g for 100 to 37% states of charge, respectively. A conventional Tafel polarization method cannot be applied for the porous metal hydride system due to the presence of internal mass-transfer effects and internal ohmic voltage drop of the electrode.

Acknowledgment

Financial support by the Office of Research and Development under Contract No. 93-F148100-000 is acknowledged gratefully.

Manuscript submitted June 5, 1995; revised manuscript received Oct. 4, 1995.

University of South Carolina assisted in meeting the publication costs of this article.

LIST OF SYMBOLS

A_s the exposed surface area of the electrodes, cm^{-2}
C_{H_2O} concentration of H_2O, mol cm^{-3}
C_{OH^-} concentration of OH^-, mol cm^{-3}
C_o hydrogen concentration directly beneath the surface, mol cm^{-3}
C_s the saturation value of C_o, mol cm^{-3}
D_i the effective diffusion coefficient for species i, $cm^2\ s^{-1}$
D_i' the true diffusion coefficient for species i, $cm^2\ s^{-1}$
E electrode potential, V
f frequency, Hz
F Faraday's constant, 96,487 C eq^{-1}
i current density per unit of mass, A g^{-1}
i_o exchange current density per unit of mass, A g^{-1}
j' microkinetic current density, A cm^{-2}
j_o' microkinetic exchange current density, A cm^{-2}
j macrokinetic current density, A cm^{-2}
j_o macrokinetic exchange current density, A cm^{-2}
k_+^o forward reaction constant, cm s^{-1}
k_-^o backward reaction constant, cm s^{-1}
k_{abs} absorption constant, mol $(cm^2\ s)^{-1}$
k_{ads} adsorption constant, mol $(cm^2\ s)^{-1}$
K a constant defined by Eq. 26, dimensionless
L half the electrode thickness, cm
M the total mass of the electrode, g
R gas constant, 8.314 J $(mol\ K)^{-1}$
R_p polarization resistance, Ω g
S the internal active specific surface area of the electrode, $cm^2\ cm^{-3}$
T temperature, K
u mobility, cm^2 mol/Js
x the distance, cm
Z impedance, Ω g

Greek

β symmetry factor, dimensionless
ϵ porosity of the electrode, dimensionless
η overpotential, V
θ hydrogen surface coverage, dimensionless
ρ the effective resistivity, Ω cm
ρ′ the true effective resistivity, Ω cm
τ tortuosity factor of the electrode, dimensionless
ϕ a constant defined by Eq. 41, dimensionless

Superscript

e equilibrium

Subscripts

b bulk of the electrolyte
i interface of the electrolyte/electrode
p pores of the electrode

REFERENCES

1. J. J. G. Williams, *Philips J. Res.*, **39,** Suppl.1, 1 (1984).
2. H. F. Bittner and C. C. Badcock, *This Journal*, **130,** 193C (1983).
3. *Hydrides for Energy Storage*, A. F. Andresen and A. J. Maeland, Editors, Proceeding of an International Symposium, International Association for Hydrogen Energy, Pergamon, Oxford (1978).
4. *Metal-Hydrides Systems, Fundamentals and Applications*, R. Kircheim, E. Fromm, and E. Wicke, Editors, Proceedings of the First International Symposium combining "Hydrogen in Metals" and "Metal Hydrides," Stuttgart (1988).
5. H. Yayama, K. Kuroki, K. Hirakawa, and A. Tomokiyo, *Jpn. J. Appl. Phys.*, **23,** 1619 (1984).
6. M. Ciureanu, D. H. Ryan, J. O. Ström-Olsen, and M. L. Trudeau, *This Journal*, **140,** 579 (1993).
7. M. Ciureanu, Q. Yang, D. H. Ryan, and J. O. Ström-Olsen, *ibid.*, **141,** 2430 (1994).
8. T. Sakai, H. Ishikawa, K. Oguro, C. Iwakura, and H. Yoneyama, *ibid.*, **134,** 558 (1987).
9. R. Wiswall, *Hydrogen in Metals II*, G. Alefeld and J. Volki, Editors, Chap. 5, Springer-Verlag, Berlin (1978).
10. H. Yayama, K. Hirakawa, and A. Tomokiyo, *Jpn. J. Appl. Phys.*, **25,** 739 (1986).
11. P. H. L. Notten and P. Hokkeling, *This Journal*, **138,** 1877 (1991).
12. B. V. Ratnakumar, C. Witham, B. Fultz, and G. Halpert, *ibid.*, **141,** L89 (1994).
13. L. G. Austin and H. Lerner, *Electrochim. Acta*, **9,** 1469 (1964).
14. L. G. Austin, *Trans. Faraday Soc.*, **60,** 1319 (1964).
15. C. W. Tobias and L. G. Austin, *Electrochim. Acta*, **14,** 639 (1969).
16. J. S. Newman, *Electrochemical Systems*, 2nd ed., Prentice-Hall, Englewood Cliffs, NJ (1991).
17. V. M. M. Lobo, *Handbook of Electrolyte Solutions*, Part A, pp. 1073-1092, Elsevier, New York (1989).
18. A. J. Bard and L. R. Faulkner, *Electrochemical Methods-Fundamentals and Applications*, p. 29, John Wiley & Sons, Inc., New York (1980).
19. T. Ikeya, K. Kumai, and T. Iwahori, *This Journal*, **140,** 3082 (1993).
20. N. Kuriyama, T. Sakai, H. Miyamura, I. Uehara, and H. Ishikawa, *J. Alloys Compounds*, **202,** 183 (1993).
22. P. A. Allen and A. Hickling, *Trans. Faraday Soc.*, **53,** 1626 (1957).